PHYSICS

Special Topic: Uncovering the Mechanism of Nickelate Superconductors

Imaging the Meissner effect in pressurized bilayer nickelate with integrated multi-parameter quantum sensor

Junyan Wen^{1,2,†}, Yue Xu^{1,2,†}, Gang Wang^{1,2,†}, Ze-Xu He^{1,2}, Yang Chen¹, Ningning Wang ^{1,2}, Tenglong Lu ¹, Xiaoli Ma^{1,2}, Feng Jin^{1,2}, Liucheng Chen¹, Miao Liu¹, Jing-Wei Fan³, Xiaobing Liu⁴, Xin-Yu Pan^{1,2,5}, Gang-Qin Liu^{1,2,5,*}, Jinguang Cheng^{1,2,*} and Xiaohui Yu^{1,2,*}

ABSTRACT

Recent reports on the signatures of high-temperature superconductivity with a critical temperature (T_c) close to 80 K have triggered great research interest and extensive follow-up studies. Although zero resistance has been successfully achieved under improved hydrostatic pressure conditions, the Meissner effect of $La_3Ni_2O_{7-\delta}$ under high pressure remains controversial. Here, using shallow nitrogen-vacancy centers implanted on the culet of diamond anvils as in situ quantum sensors, we observe compelling evidence for the Meissner effect in polycrystalline bilayer nickelate samples: magnetic field expulsion during both field-cooling and field-warming processes. In particular, we explore the multi-parameter measurement capacity of the diamond quantum sensors to extract the weak demagnetization signal of $La_3Ni_2O_{7-\delta}$. The correlated measurements of Raman spectra and magnetic imaging indicate an incomplete structural transformation related to the displacement of oxygen ions emerging in the non-superconducting region. Our work clarifies the controversy about the Meissner effect of $La_3Ni_2O_{7-\delta}$ and contributes to the development of quantum sensing of weak signals under high-pressure conditions.

Keywords: quantum metrology, nickelates, high-temperature superconductivity, Meissner effect, high pressure

INTRODUCTION

Since superconductivity has been observed in $Nd_{1-x}Sr_xNiO_2$ thin films, the study of nickelate superconductors has attracted substantial attention in the condensed matter physics community [1–5]. Notably, pressure plays a significant role in regulating the superconductivity of nickelates. It has been shown that the critical temperature (T_c) of $Pr_{0.82}Sr_{0.18}NiO_2$ thin films can be significantly increased to \sim 31 K by applying hydrostatic pressure up to 12 GPa [6]. Recent studies have observed signatures of high-temperature superconductivity (HTSC) in pressurized single crystals of $La_3Ni_2O_{7-\delta}$, with an onset T_c of about 78 K,

exceeding the McMillan limit and indicating a potential new class of HTSC at liquid nitrogen temperatures [7]. This significant discovery rapidly garnered widespread attention within the superconductivity research community [8–12]. With improved hydrostaticity, zero resistance has been researched [13–15], and angle-resolved photoemission spectroscopy (ARPES) [16,17] and optical conductivity [10] have been used to characterize its electronic properties. Meanwhile, resonant inelastic X-ray scattering (RIXS) [18], muon-spin relaxation (μ SR) [19,20] and nuclear magnetic resonance (NMR) [21] have been used to reveal the pressure-driven transition of spin-density waves (SDWs) and charge-density waves (CDWs) in nickelates.

¹Beijing National Laboratory for Condensed Matter Physics and Institute of Physics, Chinese Academy of Sciences, Beijing 100190, China; ²School of Physical Sciences, University of Chinese Academy of Sciences, Beijing 100190, China; ³Department of Physics, Hefei University of Technology, Hefei 230009, China; ⁴Laboratory of High Pressure Physics and Material Science, School of Physics and Physical Engineering, Qufu Normal University, Qufu 273165, China and ⁵CAS Center of Excellence in Topological Quantum Computation, University of Chinese Academy of Sciences, Beijing 100190, China

*Corresponding authors. E-mails: gqliu@iphy.ac.cn; jgcheng@iphy.ac.cn; yuxh@iphy.ac.cn

†Equally contributed to this work.

Received 4 June 2025; Accepted 17 June 2025

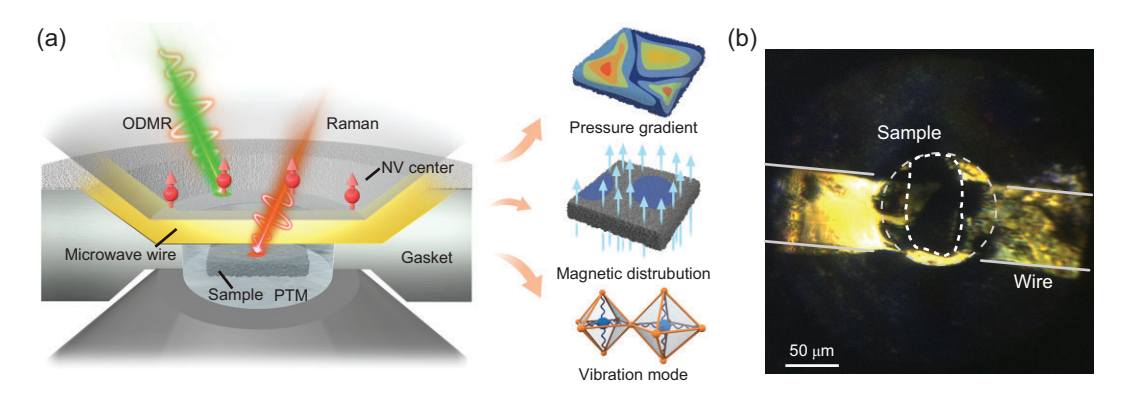


Figure 1. Correlated characterization of $La_3Ni_2O_{7-\delta}$ in DACs. (a) The $La_3Ni_2O_{7-\delta}$ and $La_2PrNi_2O_7$ samples are wrapped in the pressure transmitting medium (PTM; silicone oil or KBr) inside the DAC sample chamber. Correlated measurements of NV-based quantum sensing and Raman spectra are performed to reveal the pressure gradient, magnetic distribution and vibration mode of the samples. This provides a direct method to study the Meissner effect of superconductors under pressure. For *in situ* magnetic field and pressure measurement, diamond anvils ([111]-crystal cut) with a layer of shallow NV centers are used, and a gold antenna is placed between the anvil culet and the PTM to transmit the microwave signal. (b) Bright-field image of the diamond culet after loading sample A with 20 GPa. The sample is outlined by a white dashed line.

In contrast to the extensive and unambiguous evidence of its electronic properties, the final criterion of superconductivity, the Meissner effect, remains controversial for $La_3Ni_2O_{7-\delta}$ under pressure [7,22]. Using modulated ac susceptibility measurements, Zhou et al. found that the relative superconducting volume fraction in La₃Ni₂O₇ is only 0.68%, suggesting that the superconductivity in this nickelate is filamentary-like [23]. Using superconducting quantum interference device (SQUID) magnetometry, Li et al. reported that the maximum superconducting volume fraction of La₃Ni₂O₇ at 22.0 GPa reaches 62.7%, suggesting the bulk nature of superconductivity [24]. Such a large difference in superconducting volume fraction may result from a mixture of La₃Ni₂O₇ and other phases such as La₄Ni₃O₁₀ and La₂NiO₄. Indeed, using multi-slice electron ptychography and electron energy-loss spectroscopy, Li et al. found considerable inhomogeneity of oxygen content within the sample [25]. By replacing one-third of the La with Pr, Wang et al. demonstrated that the trilayer phase can be significantly suppressed, resulting in a superconducting volume fraction up to 97% in La₂PrNi₂O₇ [26]. Accordingly, it is important to reexamine the Meissner effect of the bilayer nickelate La₃Ni₂O₇.

In this work, we adapt the newly developed quantum sensing techniques with nitrogen-vacancy (NV) centers integrated into the diamond anvil cells (DACs) [27–32], assisted by correlated Raman spectra, to image the Meissner effect of bilayer nickelate under high pressure. With the spatially resolved magnetic field imaging around the nickelate samples, clear magnetic field expulsion effects are observed on a scale of tens of micrometers,

indicating the bulk nature of superconductivity. In particular, to extract the weak demagnetization signal from the pressure-sensitive La₃Ni₂O₇ sample, we explore the multi-parameter measurement capacity of the NV center and demonstrate the simultaneous imaging of pressure and magnetic field under high pressures. The correlated measurements of Raman spectra and NV-based magnetic imaging indicate an incomplete structural transformation related to the displacement of oxygen ions emerging in the non-superconducting region. Our results provide crucial evidence for the Meissner effect in pressurized bilayer nickelate superconductors and contribute both to the mechanistic understanding of their HTSC and to the development of NV-based quantum sensing under high-pressure conditions.

RESULTS

As shown in Fig. 1a, the high-pressure sample chamber consists of two diamond anvils and a gasket. Through the transparent diamond window, optically detected magnetic resonance (ODMR) and Raman spectra can be measured under high pressure, in a correlated manner. To investigate the magnetic field and stress distribution around the superconducting samples, shallow NV centers are created on one of the diamond culets by nitrogen ion implantation (20 keV, 2×10^{14} cm⁻²) and subsequent high temperature annealing (800°C, 2 h). The spin resonance frequencies of an NV center are sensitive to the local magnetic field (and also to pressure, temperature and so on) and can be read out optically, providing a convenient and efficient method to study magnetic properties inside DACs.

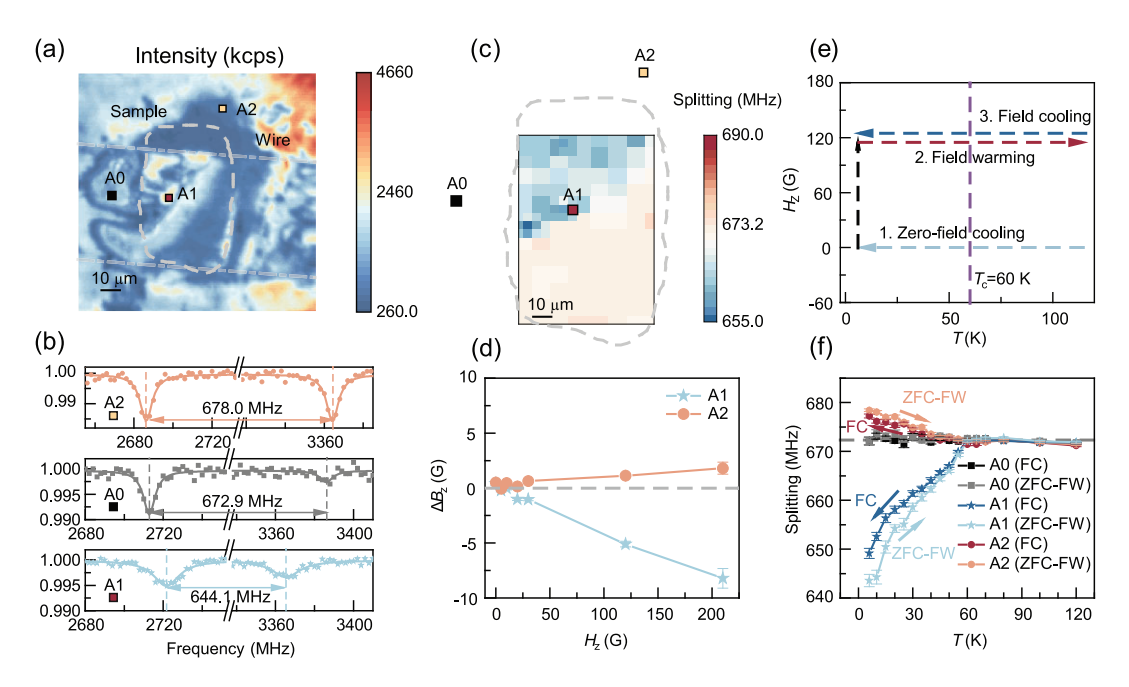


Figure 2. Local diamagnetism in $La_2PrNi_2O_7$ at 20 GPa. (a) Fluorescence image of sample A ($La_2PrNi_2O_7$ in silicon oil). The edge of the sample is outlined with a gray dashed line. The unit of the fluorescence intensity is kilo counts per second (kcps). (b, c) Typical ODMR spectra of the NV centers (b) and magnetic field mapping (c) under an external magnetic field of $H_Z \sim 120$ G after ZFC of the sample to 7 K. Three points (A0, A1, A2) are selected based on their position with respect to the $La_2PrNi_2O_7$ sample. Point A1 is directly on the sample, A2 is at the edge of the sample and A0 is far away from the sample (serves as a reference point). The blue area in (c) shows the local diamagnetism (these points have smaller ODMR splitting than that of the reference point). (d) Local magnetic field at the NV positions as a function of the applied external magnetic field (after ZFC). For the NV centers at point A1, their local magnetic field is about 5% smaller than the applied external magnetic field. In sharp contrast, the NV centers at point A2 feel an enhanced local magnetic field. (e) Measurement protocol of ZFC-FW and FC. (f) ODMR splitting of three selected points under 120 G ZFC-FW and FC measurements. The combination of the ZFC-FW and FC curves provide clear evidence of the Meissner effect.

Details of the ODMR technique can be found in the Methods and previous work [29,33].

The Meissner effect of La₂PrNi₂O₇ and La₃Ni₂O_{7-δ} polycrystalline samples was studied using diamond quantum sensors, in conjunction with in situ Raman measurements. For sample A, La₂PrNi₂O₇ in liquid pressure-transmitting medium (silicon oil), ODMR spectra were measured under different pressures and external magnetic fields. We also performed experiments with La₂PrNi₂O₇ (sample B) in a solid pressure-transmitting medium (KBr) to investigate the influence of hydrostatic pressure conditions on superconductivity. Correlated Raman and ODMR measurements were performed on sample B to determine the structural distinctions on both the superconducting and non-superconducting regions. Finally, sample C, $La_3Ni_2O_{7-\delta}$ in silicon oil, was measured. Since the diamagnetism signal of this La₃Ni₂O_{7-\delta} sample is weak and buried in the pressure gradient background, we performed additional zero-field ODMR measurements to extract and decouple the contribution of local stress, and successfully obtained the diamagnetism image of the La₃Ni₂O_{7- δ} sample.

Local diamagnetism in La₂PrNi₂O₇

We start with the sample of La₂PrNi₂O₇ in silicon oil (sample A) at 20 GPa. As shown in Figs 1b and 2a, the sample edge and its relative position on the diamond culets were determined by comparing the bright-field image and the confocal NV fluorescence image; see Fig. S1 for more details. Figure 2b shows typical ODMR spectra of NV centers near the sample. These spectra were measured under an external magnetic field of around 120 G after zero-field cooling the sample to 6 K. The strength of the external magnetic field was calibrated using the ODMR splitting of the NV centers away from the sample (point A0 in Fig. 2a). For NV centers directly above the sample, e.g. at point A1, the ODMR splitting (644.1 MHz) is noticeably smaller than that of the reference point (672.9 MHz), indicating local diamagnetism of the La₂PrNi₂O₇ sample. At the same time, a relatively larger splitting (678.0 MHz) was observed at point A2, which was due to the magnetic flux concentration at the sample edge. By measuring more points around the sample, a superconducting region can be identified, as shown by the blue color in Fig. 2c. For the measured region

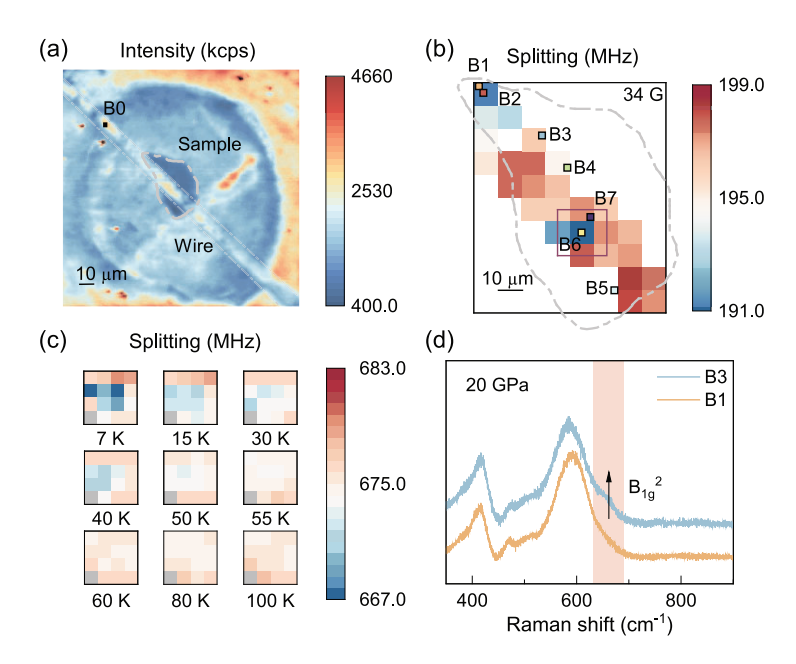


Figure 3. Correlated magnetic and Raman measurements of $La_2PrNi_2O_7$ under pressure. (a) Fluorescence image of sample B ($La_2PrNi_2O_7$ in KBr). The edge of the sample is outlined with a black dashed line. (b) Magnetic field mapping under an external magnetic field of $H_Z=34$ G after ZFC of the sample to 7 K. The blue region exhibits a noticeable diamagnetism. *In situ* Raman measurements are performed on the superconducting regions (B1, B2) and the non-superconducting regions (B3, B5) under different pressures. (c) Magnetic field mapping of one of the superconducting regions [position of purple square marked in (b)] during the FW process; the external magnetic field is around 120 G. Above the critical temperature T_c , the local diamagnetism disappears and all NV centers feel the uniform external magnetic field. The region on the gray square shows a feeble contrast to fit the ODMR splitting. (d) The Raman spectra of B1 and B3 at 20 GPa. As shown in the figure, a small satellite peak is observed in the non-superconducting region (B3) at 20 GPa, while it is suppressed in the superconducting region (B1). This peak is also presented at atmospheric pressure before compression (shown in Fig. S6a).

of $110~\mu m \times 74.5~\mu m$, about two-fifths of the points show diamagnetism, indicating a relatively large amount of superconducting shielding volume in the $La_2PrNi_2O_7$ sample. In addition, Fig. 2d presents diamagnetism (at point A1) and flux concentration effects (at point A2) under different external magnetic fields, which show an almost linear dependence in all measured magnetic fields.

To further verify the Meissner effect of the $La_2PrNi_2O_7$ sample, more ODMR spectra were acquired during zero-field-cooling field-warming (ZFC-FW) and field-cooling (FC) processes, with an external magnetic field of 120 G. The detailed experimental protocol is shown in Fig. 2e. As displayed in Fig. 2f, both the diamagnetism (at point A1) and the flux concentration (at point A2) show a clear temperature dependence. In comparison, the reference point (A0) remains almost constant splitting throughout the ZFC-FW and FC processes. From these results, a superconducting transition temperature of $T_c \sim 60$ K is obtained and the expul-

sion of magnetic flux throughout the FC process, an intrinsic property of the Meissner effect, is observed. Meanwhile, compared to the ZFC-FW process, a weaker diamagnetism effect was observed at point A1 during the FC process, which can be attributed to the flux trapping effect [31].

To rule out the possibility that the diamagnetism originates from other magnetic impurities, both the ZFC-FW and FC measurements were performed under an external magnetic field of opposite direction and a strength of about -210 G (see Fig. 2e for the experimental protocol). The diamagnetism effect and its temperature dependence are similar to those observed at 120 G (shown in Fig. S2), indicating that the local diamagnetism sensed by the NV centers is not due to the compensating effect of local magnetic impurities in or near the samples. In addition, we varied the pressure from 11 to 30 GPa and performed ZFC-FW measurements. The reduced diamagnetic strength at pressures above 20 GPa indicates that superconductivity is gradually suppressed by the pressure (shown in Fig. S3). The T_c values determined from the ODMR measurements are included in the phase diagram in Fig. S3d. After the pressure decreased to 11 GPa, the effect of diamagnetism disappeared, which is consistent with the electrical resistance results in the previous study [26].

Simultaneous magnetic and Raman measurements

To investigate the effects of pressure-transmitting media, another La₂PrNi₂O₇ sample (sample B) was loaded in KBr (a solid pressure-transmitting medium) and compressed to 30 GPa. We then characterized the sample with both ODMR and Raman measurements. As shown in Fig. 3a, the confocal image clearly shows the shape and relative position of the sample, the microwave wire, and the edge of the sample chamber. Figure 3b shows a magnetic field image under an external magnetic field of about 34 G after zero-field cooling of the sample to 7 K. The test area of this sample is limited to the area next to the microwave antenna to maintain a good ODMR contrast at low microwave power. Local diamagnetism (reduction of ODMR splitting) was observed in two regions of the sample. The local diamagnetism of one region was tracked during the field-warming (FW) process (under an external magnetic field of around 120 G), as shown in Fig. 3c. As the temperature increases to T_c , the diamagnetic effect gradually fades out. When the temperature is above T_c , the entire region exhibits a uniform magnetic field in line with the strength

at reference point B0. More results of the ZFC-FW measurement in sample B can be found in Fig. S4. Compared to sample A, the diamagnetism effect in sample B is smaller. This is plausible because a liquid pressure-transmitting medium (silicon oil) was used in sample A, therefore a better hydrostatic condition was obtained. As a result, a larger superconducting volume and more pronounced diamagnetism were observed in sample A. These results are consistent with the previous studies on the electrical resistance [7,13,14,34].

Thanks to the high spatial resolution of the NV-based magnetometer, the distribution of the superconducting regions is visually obtained, which enables us to perform targeted spectroscopic measurements. We then used the *in situ* Raman spectrum to study the structure of pressurized La₂PrNi₂O₇ in both the superconducting and non-superconducting regions, which are marked in Fig. 3b. As shown in Fig. 3d and Fig. S5b, a slight difference is observed in the Raman spectra, where a satellite peak around $680~{\rm cm}^{-1}$ is suppressed in the superconducting region at 20 GPa. The satellite peak is more pronounced in the non-superconducting region and in the sample before compression (see Fig. S6a).

Our density-functional perturbation theory (DFPT) calculations show that structural transformations in La₃Ni₂O₇ manifest as degeneracy of Raman peaks. When La₃Ni₂O₇ is compressed from 0 GPa to about 9 GPa, the difference between the B_{2g} and B_{1g}² modes gradually becomes negligible, and a single mode (Eg) appears under high pressures, as shown in Fig. S6b. The same phenomenon is observed for Pr₃Ni₂O₇ (Fig. S6c), implying that the above discussion may reflect the common feature of this class of materials. Indeed, a similar phenomenon has been observed for the bilayer Ruddlesden-Popper (R-P) perovskite Li₂CaTa₂O₇, which has a similar structure to $La_2PrNi_2O_7$ [35]. A comparison with the Raman spectra of related compounds [36] shows that the satellite peak in La₂PrNi₂O₇ can be assigned to an oxygen B_{1g} mode. Therefore, the satellite peak in the non-superconducting region may be attributed to the incomplete structural transformation caused by the displacements of the oxygen ions, which is challenging to be observed in X-ray and neutron diffraction [37]. These results are well consistent with the change of the bond angle of the Ni-O-Ni in La₃Ni₂O₇. In the case of La₃Ni₂O₇, the emergence of HTSC is seen along with the structural transformations from Amam to Fmmm with the change of the bond angle of the Ni-O-Ni from 168.0° to 180° along the c-axis [34]. As a consequence, the electronic interactions within the bilayer of NiO2 are increased, corresponding to the metallization of the inter-layer

 σ -bonding bands. This phenomenon is observed in the conventional high- T_c superconductors, such as MgB₂ and Li₃B₄C₂ [7].

Local diamagnetism imaging in $La_3Ni_2O_{7-\delta}$

To investigate the Meissner effect of La₃Ni₂O_{7– δ}, a polycrystalline sample was loaded with silicon oil as the pressure-transmitting medium (sample C). Figure 4a shows the confocal image of NV fluorescence when the sample is compressed to 20 GPa. Following the experimental protocols shown in Fig. 2e, the ZFC-FW and FC measurements were performed under an external magnetic field of around 120 G. As shown in Fig. 4b, local diamagnetism was observed during both the FW and FC processes. However, the diamagnetism signal (change of ODMR splitting below and above T_c) in sample C is only one-fifth of sample A, indicating a relatively small superconducting volume in this sample.

Notably, there are obvious differences of ODMR splitting among different NV centers, even when the temperature is above $T_{\rm c.}$ This phenomenon can be explained by the inhomogeneous distribution of stress on the diamond culet. In particular, the compressive stress can shift the center frequency of the ODMR spectra, while the differential stress regulates the ODMR splitting. It is worth noting that this phenomenon also occurs in the former two samples, but the contribution of stress is much weaker compared to the contribution of the superconducting diamagnetism effect in these two samples. Fortunately, diamond NV centers can also serve as in situ stress sensors. To decouple the contribution of stress, we perform ODMR measurements at 150 K (above T_c) in zero field (see Supplementary data for details). As shown in Fig. 4c and d, the maximum pressure variance among the sample is about 3 GPa. With this in hand, we can eliminate the influence of non-uniform stress distribution and obtain a strain-free magnetism distribution, as shown in Fig. 4e. In short, the Meissner effect of La₃Ni₂O_{7-δ} was imaged with NV centers under high pressure.

Finally, the diamagnetism signals of three samples during ZFC-FW are normalized and compared with each other. As shown in Fig. 4f, it can be clearly seen that pressurized La₂PrNi₂O₇ in silicon oil exhibits the strongest diamagnetism effect, while La₂PrNi₂O₇ in KBr has a relatively weaker signal, indicating that the hydrostatic conditions play an important role in achieving a high superconducting volume fraction. Overall, La₃Ni₂O_{7- δ} in silicon oil has the weakest signal, which is consistent with its inhomogeneous nature (mixture of La₃Ni₂O₇ and other phases such as La₄Ni₃O₁₀ and La₂NiO₄) [24,25].

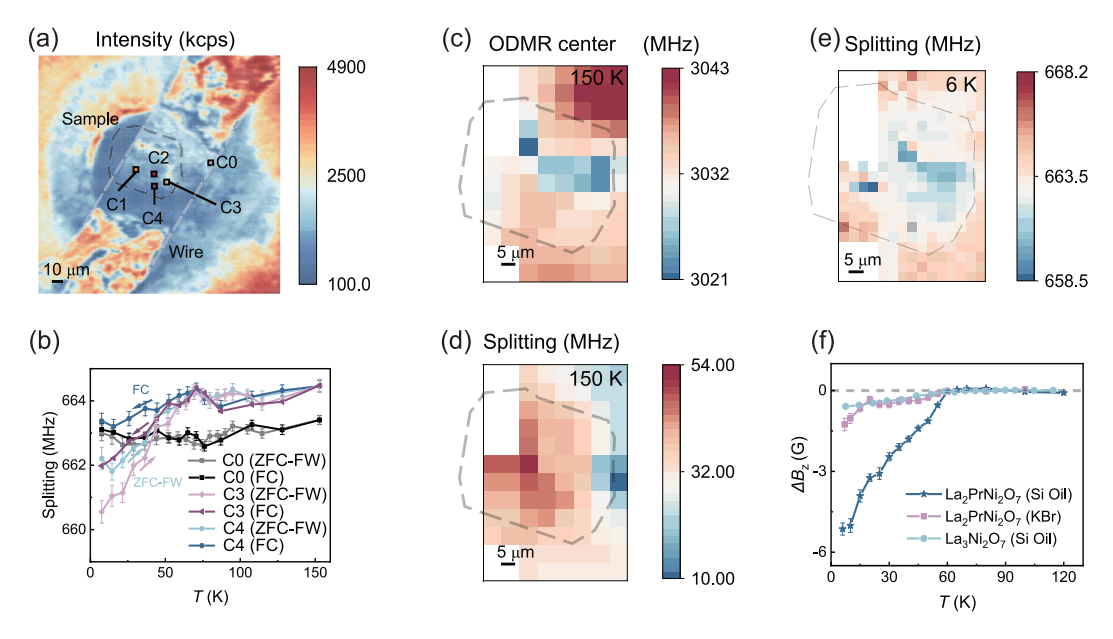


Figure 4. Magnetic and stress measurement of the La₃Ni₂O_{7- δ} sample at 20 GPa. (a) Fluorescence image of sample C (La₃Ni₂O_{7- δ} in silicon oil). The edge of the sample is outlined by the black dashed line. (b) ODMR splitting of the NV centers during the ZFC-FW and FC processes, with an external magnetic field of around 120 G. The NV positions are marked in (a). Both the diamagnetism of the La₃Ni₂O_{7- δ} sample and the local stress contribute to the ODMR splitting. (c, d) Stress distribution revealed by the zero-field ODMR spectra at 150 K (> T_c). The center frequency of the ODMR spectra (c) reveals the compressive stress, while the splitting of the ODMR spectra (d) is proportional to the differential stress. (e) Magnetic image under an external magnetic field of around 120 G after ZFC. Note that the contribution of the stress distribution has been subtracted by the results shown in (c and d). The region on the gray square is an odd point and is therefore not included in the discussion. (f) Comparison of the diamagnetism effect of the three samples during ZFW-FW measurement. The external magnetic field is around 120 G. For each point, the ODMR splitting at high temperatures (> T_c) is used as the reference to calculate ΔB_7 .

DISCUSSION

It is noteworthy that the superconducting diamagnetism observed in our work exhibits a weaker magnitude compared to other superconducting systems (e.g. cuprate and hydride superconductors). We attribute this weaker diamagnetic response primarily to the limited superconducting volume fraction in the measured nickelate samples. The same situation has occurred in previous electrical and magnetic measurements of nickelate, which have consistently reported relatively weak superconducting signals with pronounced sample inhomogeneity [7,11,13,14,26]. Although there is no perfect diamagnetic signal, the characteristic field-dependent magnetic response and the expulsion of magnetic flux during FC measurements clearly confirm the presence of the Meissner effect in pressurized bilayer nickelate.

In conclusion, the Meissner effect is imaged in pressurized bilayer nickelate superconductors $La_3Ni_2O_{7-\delta}$ and $La_2PrNi_2O_7$ using NV center quantum sensors. By combining ZFC-FW measurements with FC measurements in different external magnetic fields, our results confirm the

existence of HTSC in La₃Ni₂O_{7- δ} and La₂PrNi₂O₇. Through the correlated measurement between ODMR and Raman spectroscopy, we identify the structural difference between superconducting and non-superconducting regions in the La₂PrNi₂O₇ sample. These measurements indicate that the inhomogeneous superconductivity may be due to the incomplete structural transformations related to the displacement of oxygen ions on the non-superconducting regions and the complete transformations on the superconducting regions, which helps us to understand the underlying mechanism in nickelate high-temperature superconductors.

Our research demonstrates that the diamond NV center is a powerful probe to study inhomogeneous samples under high pressure, due to their high sensitivity, high spatial resolution and multi-parameter sensing capacity. When measuring samples with weak magnetic signals under high pressure, the influence of the stress gradient is a critical issue that should be given sufficient attention. With spatially resolved ODMR measurement, various *in situ* high-pressure experiments, such as Raman and absorption spectroscopy, can be performed

efficiently. Our work not only demonstrates the feasibility of using NV center sensors to measure weak magnetic signals under high pressure but also provides a detailed experimental methodology.

SUPPLEMENTARY DATA

Supplementary data are available at NSR online.

ACKNOWLEDGEMENTS

We thank the high-pressure synergetic measurement station of the Synergetic Extreme Condition User Facility for the help with high-pressure Raman measurements.

FUNDING

This work was supported by the National Key R&D Program of China (2023YFA1608900, 2024YFA1611300, 2021YFA1400300, 2019YFA0308100, 2023YFA1406100 and 2021YFA1400200), the National Natural Science Foundation of China (12375304, 12404163, 12022509, T2121001, 12025408, 12404179, 12074422 and 12374468), the Beijing Natural Science Foundation (Z200009 and Z230005), the Innovation Program for Quantum Science and Technology (2023ZD0300600) and the Strategic Priority Research Program of CAS (XDB33000000).

AUTHOR CONTRIBUTIONS

G.Q.L., J.G.C. and X.H.Y. designed and supervised this project. G.W., N.N.W. and J.G.C. synthesized and provided the samples; J.W.F. implanted NV centers into the diamond culets; J.Y.W. loaded the samples into high-pressure chambers; Y.X., Z.X.H. and C.Y. conducted the ODMR measurements; J.Y.W., X.L.M., F.J. and L.C.C. measured the *in situ* high-pressure and low-temperature Raman spectra; J.Y.W., Y.X., Z.X.H., C.Y., G.Q.L and X.H.Y. analyzed all the collected data; T.L.L. and M.L. performed DFPT calculations and gave advice from a theoretical perspective; J.Y.W., G.Q.L., J.G.C. and X.H.Y. wrote the paper with inputs from all coauthors.

Conflict of interest statement. None declared.

REFERENCES

- Li D, Lee K, Wang BY et al. Superconductivity in an infinite-layer nickelate. Nature 2019; 572: 624

 –7.
- Zeng S, Tang CS, Yin X et al. Phase diagram and superconducting dome of infinite-layer Nd_{1-x}Sr_xNiO₂ thin films. Phys Rev Lett 2020; 125: 147003.
- Zeng S, Li C, Chow LE et al. Superconductivity in infinite-layer nickelate La_{1-x}Ca_xNiO₂ thin films. Sci Adv 2022;8: eabl9927.
- 4. Ding X, Tam CC, Sui X *et al.* Critical role of hydrogen for superconductivity in nickelates. *Nature* 2023; **615**: 50–5.
- Osada M, Wang BY, Lee K et al. Phase diagram of infinite layer praseodymium nickelate Pr_{1-x}Sr_xNiO₂ thin films. Phys Rev Mater 2020;4: 121801.

- Wang NN, Yang MW, Yang Z et al. Pressure-induced monotonic enhancement of T_c to over 30 K in superconducting Pr_{0.82}Sr_{0.18}NiO₂ thin films. Nat Commun 2022; 13: 4367.
- Sun H, Huo M, Hu X et al. Signatures of superconductivity near 80 K in a nickelate under high pressure. Nature 2023; 621: 493– 8
- Christiansson V, Petocchi F, Werner P et al. Correlated electronic structure of La₃Ni₂O₇ under pressure. Phys Rev Lett 2023; 131: 206501.
- 9. Zhang Y, Lin L-F, Moreo A *et al.* Structural phase transition, s_{\pm} -wave pairing, and magnetic stripe order in bilayered superconductor La₃Ni₂O₇ under pressure. *Nat Commun* 2024; **15**: 2470.
- Liu Z, Huo M, Li J et al. Electronic correlations and partial gap in the bilayer nickelate La₃Ni₂O₇. Nat Commun 2024; 15: 7570.
- 11. Zhu Y, Peng D, Zhang E *et al.* Superconductivity in pressurized trilayer La₄Ni₃O₁₀₋₈ single crystals. *Nature* 2024; **631**: 531–6.
- 12. Wang L, Li Y, Xie S-Y *et al.* Structure responsible for the superconducting state in La₃Ni₂O₇ at high-pressure and low-temperature conditions. *J Am Chem Soc* 2024; **146**: 7506–14.
- Hou J, Yang P-T, Liu Z-Y et al. Emergence of high-temperature superconducting phase in pressurized La₃Ni₂O₇ crystals. Chin Phys Lett 2023; 40: 117302.
- Zhang Y, Su D, Huang Y et al. High-temperature superconductivity with zero resistance and strange-metal behaviour in La₃Ni₂O_{7-δ}. Nat Phys 2024; 20: 1269–73.
- 15. Wang G, Wang NN, Shen XL *et al.* Pressure-induced superconductivity in polycrystalline $La_3Ni_2O_{7-\delta}$. *Phys Rev X* 2024; **14**: 011040.
- Yang J, Sun H, Hu X et al. Orbital-dependent electron correlation in double-layer nickelate La₃Ni₂O₇. Nat Commun 2024; 15: 4373
- Abadi S, Xu K-J, Lomeli EG et al. Electronic structure of the alternating monolayer-trilayer phase of La₃Ni₂O₇. Phys Rev Lett 2025; 134: 126001.
- Xie T, Huo M, Ni X et al. Strong interlayer magnetic exchange coupling in La₃Ni₂O_{7-δ} revealed by inelastic neutron scattering. Sci Bull 2024: 69: 3221–7.
- 19. Khasanov R, Hicken TJ, Gawryluk DJ *et al.* Pressure-enhanced splitting of density wave transitions in La₃Ni₂O_{7 $-\delta$}. *Nat Phys* 2025; **21**: 430-6.
- Chen K, Liu X, Jiao J et al. Evidence of spin density waves in La₃Ni₂O₇₋₈. Phys Rev Lett 2024; 132: 256503.
- 21. Zhao D, Zhou Y, Huo M *et al.* Pressure-enhanced spin-density-wave transition in double-layer nickelate La₃Ni₂O_{7– δ}. *Sci Bull* 2025; **70**: 1239–45.
- 22. Puphal P, Reiss P, Enderlein N *et al.* Unconventional crystal structure of the high-pressure superconductor La₃Ni₂O₇. *Phys Rev Lett* 2024; **133**: 146002.
- 23. Zhou Y, Guo J, Cai S *et al.* Investigations of key issues on the reproducibility of high- T_c superconductivity emerging from compressed La₃Ni₂O₇. *Matter Radiat Extremes* 2025; **10**: 027801.
- 24. Li J, Peng D, Ma P *et al.* Identification of the superconductivity in bilayer nickelate La₃Ni₂O₇ upon 100 GPa. *Natl Sci Rev* 2025; **12**: nwaf220.

- Dong Z, Huo M, Li J et al. Visualization of oxygen vacancies and self-doped ligand holes in La₃Ni₂O_{7—8}. Nature 2024; 630: 847–52.
- Wang N, Wang G, Shen X et al. Bulk high-temperature superconductivity in pressurized tetragonal La₂PrNi₂O₇. Nature 2024; 634: 579–84.
- Hsieh S, Bhattacharyya P, Zu C et al. Imaging stress and magnetism at high pressures using a nanoscale quantum sensor. Science 2019; 366: 1349–54
- Lesik M, Plisson T, Toraille L et al. Magnetic measurements on micrometersized samples under high pressure using designed NV centers. Science 2019; 366: 1359–62.
- Shang Y-X, Hong F, Dai J-H et al. Magnetic sensing inside a diamond anvil cell via nitrogen-vacancy center spins. Chin Phys Lett 2019; 36: 086201.
- Yip KY, Ho KO, Yu KY et al. Measuring magnetic field texture in correlated electron systems under extreme conditions. Science 2019; 366: 1355–59.
- Bhattacharyya P, Chen W, Huang X et al. Imaging the Meissner effect in hydride superconductors using quantum sensors. Nature 2024; 627: 73–9.

- 32. Wang M, Wang Y, Liu Z *et al.* Imaging magnetism evolution of magnetite to megabar pressure range with quantum sensors in diamond anvil cell. *Nat Commun* 2024: **15**: 1.
- 33. Dai J-H, Shang Y-X, Yu Y-H *et al.* Optically detected magnetic resonance of diamond nitrogen-vacancy centers under megabar pressures. *Chin Phys Lett* 2022; **39**: 117601.
- 34. Wang M, Wen H-H, Wu T *et al.* Normal and superconducting properties of La₃Ni₂O₇. *Chin Phys Lett* 2024; **41**: 077402.
- 35. Galven C, Mounier D, Bouchevreau B *et al.* Phase transitions in the Ruddlesden–Popper Phase Li₂CaTa₂O₇: X-ray and neutron powder thermodiffraction, TEM, Raman, and SHG experiments. *Inorg Chem* 2016; **55**: 2309–23.
- 36. Dias A, Viegas JI, Moreira, RL. Synthesis and μ -Raman scattering of Ruddlesden-Popper ceramics $Sr_3Ti_2O_7$, $SrLa_2Al_2O_7$ and $Sr_2LaAlTiO_7$. *J Alloys Compd* 2017; **725**: 77–83.
- 37. Adler P, Goncharov AF, Syassen K *et al.* Optical reflectivity and Raman spectra of Sr_2FeO_4 under pressure. *Phys Rev B* 1994; **50**: 11396–402.